International Journal of Thermophysics, Vol. 28, No. 3, June 2007 (© 2007)
DOI: 10.1007/s10765-007-0209-8

Density and Surface Tension of Electromagnetically Levitated Cu–Co–Fe Alloys

J. Brillo[1,2] **and I. Egry**[1]

The density and surface tension of Cu–Co–Fe alloys have been measured using the non-contact technique of electromagnetic levitation. At temperatures above and below the liquidus point, the density and surface tension are linear functions of temperature. The experimental density results can be predicted by means of the regular solution model from the binary phases alone, i.e., no assumption about ternary interactions needs to be made. The surface tension values are in good agreement with numerical solutions of the Butler equation if the known Gibbs excess energies are used. It is found that, for Cu–Co–Fe, it is possible to predict the surface tension from the binary systems as well. In addition to this, the surface tension is insensitive to substitution of the two transition metals, Co and Fe.

KEY WORDS: Butler equation; copper–cobalt–iron alloys; density; electromagnetic levitation; liquid metals; surface tension.

1. INTRODUCTION

Copper-based multicomponent alloys play an important role in many technical applications. For instance, the Cu–Co–Fe alloy has become an interesting candidate for the development of magnetic sensors based on the giant magnetoresistance (GMR) effect [1–4].

Despite their technical importance, there is still a lack of information and understanding of the thermophysical properties of these (multicomponent) alloys. At present, data for liquid copper-based alloys are available for some binary systems only [5–7].

[1] Deutsches Zentrum für Luft- und Raumfahrt, Institut für Materialphysik im Weltraum Köln 51147, Germany.
[2] To whom correspondence should be addressed. E-mail: Juergen.Brillo@dlr.de

Recently, we investigated the density and surface tension of the Cu–Ni–Fe ternary system [8,9]. The present work focuses on Cu–Co–Fe and addresses the question whether or not it is possible to predict the density and surface tension of the ternary alloy from the properties of the binary phases.

The Cu–Co–Fe system serves as a model system for monotectic ternary alloys in general [10–13]. It combines a good conductor (Cu) with a strong magnet (Co and Fe); its phase diagram is characterized by a flat liquidus surface and by a broad metastable miscibility gap reaching from the Cu–Co binary to the Cu–Fe border [11,13].

Generally, the molar volume, V, of a solution with N components i, each having a bulk concentration c_i^{B} is expressed as a function of temperature and concentrations [14,15] as

$$V\left(c_1^{\mathrm{B}}, \ldots, c_N^{\mathrm{B}}, T\right) = \sum c_i^{\mathrm{B}} V_i(T) + {}^{\mathrm{E}}V\left(c_1^{\mathrm{B}}, \ldots, c_N^{\mathrm{B}}, T\right) \tag{1}$$

In this equation, V_i is the molar volume of component i, and ${}^{\mathrm{E}}V$ is the excess volume. For ${}^{\mathrm{E}}V = 0$, Eq. (1) reduces to a simple linear combination of the individual V_i.

The following expression can be used to describe the excess volume of a ternary alloy [14,15]:

$${}^{\mathrm{E}}V\left(c_1^{\mathrm{B}}, \ldots, c_3^{\mathrm{B}}, T\right) = \sum_{i}^{2} \sum_{j>i}^{3} c_i^{\mathrm{B}} c_j^{\mathrm{B}}\ {}^{\mathrm{E}}V_{i,j} + c_1^{\mathrm{B}} c_2^{\mathrm{B}} c_3^{\mathrm{B}}\ {}^{\mathrm{E}}V^{\mathrm{T}} \tag{2}$$

In Eq. (2) the parameters ${}^{\mathrm{E}}V_{i,j}$ describe the binary interaction between elements i and j and ${}^{\mathrm{E}}V^{T}$ is a parameter describing the ternary interaction. As a first approximation, ${}^{\mathrm{E}}V_{i,j}$ can be assumed independent of temperature and concentration. For Cu–Co–Fe, the binary interaction parameters ${}^{\mathrm{E}}V_{i,j}$ have been determined in a previous study [16].

It is *a priori* an open question whether or not the ternary interaction parameter ${}^{\mathrm{E}}V^{\mathrm{T}}$ can be neglected in Eq. (2). For Cu–Ni–Fe we found that a large positive ternary parameter ${}^{\mathrm{E}}V^{\mathrm{T}}$ had to be taken into account [10].

For the calculation of the surface tension from thermodynamic potentials using the Butler equation [17,18], a knowledge of the excess Gibbs free enthalpy ${}^{\mathrm{E}}G$ is required. It is usually written for a mixture in a form similar to Eq. (2); see Refs. 19, 20:

$${}^{\mathrm{E}}G\left(c_1^{\mathrm{B}}, \ldots, c_3^{\mathrm{B}}, T\right) = \sum_{i}^{2} \sum_{j>i}^{3} c_i^{\mathrm{B}} c_j^{\mathrm{B}} G_{i,j} + c_1^{\mathrm{B}} c_2^{\mathrm{B}} c_3^{\mathrm{B}} G^{\mathrm{T}} \tag{3}$$

In this equation, the $G_{i,j}$ are binary interaction parameters and G^{T} is a parameter describing the ternary interaction. Both the binary and ternary parameters depend on temperature and concentration. Conveniently, the $G_{i,j}$ are expressed by the Redlich–Kister equation in the following form [19,20]:

$$G_{i,j} = \sum_{\nu=0} {}^{\nu}L_{i,j}\left(c_i^{\mathrm{B}} - c_j^{\mathrm{B}}\right)^{\nu} \tag{4}$$

The parameter ${}^{\nu}L_{i,j}$ depends on temperature, but not on concentration. For the present system, Cu–Co–Fe, numerical values for ${}^{\nu}L_{i,j}$ published in Refs. 12 and 21 are used.

In order to describe the miscibility gap of Cu–Co–Fe correctly, Bamberger showed that the ternary parameter had to be written as follows [12]:

$$G^{\mathrm{T}} = \left(-80c_{\mathrm{Cu}}^{\mathrm{B}} + 5c_{\mathrm{Co}}^{\mathrm{B}} + 10c_{\mathrm{Fe}}^{\mathrm{B}}\right)\left[\mathrm{kJ}\cdot\mathrm{mol}^{-1}\right] \tag{5}$$

Once the Gibbs free enthalpy is known, the surface tension, $\gamma_{123}(T)$, of a liquid ternary alloy, consisting of three elements $i = 1, 2, 3$, with corresponding surface tensions, $\gamma_i(T)$, can be calculated by the Butler equation:

$$\begin{aligned}
\gamma_{123}(T) &= \gamma_1 + \tfrac{RT}{S_1}\ln\left(\tfrac{1-c_2^{\mathrm{S}}-c_3^{\mathrm{S}}}{1-c_2^{\mathrm{B}}-c_3^{\mathrm{B}}}\right) + \tfrac{1}{S_1}\left\{{}^{\mathrm{E}}G_1^{\mathrm{S}}\left(T, c_2^{\mathrm{S}}, c_3^{\mathrm{S}}\right) - {}^{\mathrm{E}}G_1^{\mathrm{B}}\left(T, c_2^{\mathrm{B}}, c_3^{\mathrm{B}}\right)\right\} \\
&= \gamma_2 + \tfrac{RT}{S_2}\ln\left(\tfrac{c_2^{\mathrm{S}}}{c_2^{\mathrm{B}}}\right) + \tfrac{1}{S_2}\left\{{}^{\mathrm{E}}G_2^{\mathrm{S}}\left(T, c_2^{\mathrm{S}}, c_3^{\mathrm{S}}\right) - {}^{\mathrm{E}}G_2^{\mathrm{B}}\left(T, c_2^{\mathrm{B}}, c_3^{\mathrm{B}}\right)\right\} \\
&= \gamma_3 + \tfrac{RT}{S_3}\ln\left(\tfrac{c_3^{\mathrm{S}}}{c_3^{\mathrm{B}}}\right) + \tfrac{1}{S_3}\left\{{}^{\mathrm{E}}G_3^{\mathrm{S}}\left(T, c_2^{\mathrm{S}}, c_3^{\mathrm{S}}\right) - {}^{\mathrm{E}}G_3^{\mathrm{B}}\left(T, c_2^{\mathrm{B}}, c_3^{\mathrm{B}}\right)\right\}
\end{aligned} \tag{6}$$

where R is the universal gas constant, T is the temperature, S_i is the surface area in a monolayer of pure liquid i, c_i^{B} is the mole fraction of component i in the bulk phase, and c_i^{S} is the mole fraction of component i in the surface phase. ${}^{\mathrm{E}}G_i^{\mathrm{B}}$ denotes the partial excess Gibbs energy in the bulk and ${}^{\mathrm{E}}G_i^{\mathrm{S}}$ the partial excess Gibbs energy of component i in the surface layer.

Finally, it was shown by Tanaka and Iida [18] that ${}^{\mathrm{E}}G_i^{\mathrm{S}}$ can be written as

$${}^{\mathrm{E}}G_i^{\mathrm{S}} \approx \frac{3}{4}{}^{\mathrm{E}}G_i^{\mathrm{B}} \tag{7}$$

The surface area $S_i (i = 1, 2, 3)$ is calculated from the molar volume V_i as follows [17]: $S_i = 1.091(6.02 \times 10^{23})^{1/3} V_i^{2/3}$. The partial excess Gibbs energies ${}^{\mathrm{E}}G_i^{\mathrm{B}}$ are derived from the excess Gibbs energy ${}^{\mathrm{E}}G$ by partial derivatives with respect to concentrations.

2. EXPERIMENTAL

Density and surface tension measurements were performed using an electromagnetic levitation chamber that is described in detail in Refs. 7 and 22. The sample is processed under a protective atmosphere of He/8vol%-H_2 in a levitation coil. The temperature, T, is measured by an infrared pyrometer aimed at the top of the sample.

For the determination of the density, the sample is illuminated from behind by a HeNe laser that is equipped with a beam expander. The shadow image is captured by means of a digital CCD camera and analyzed by an edge detection algorithm. The edge curve $R(\varphi)$ with R and φ being the radius and the azimuthal angle, respectively, is averaged over 1000 frames, $\langle R(\varphi)\rangle$, and it is then fitted by Legendre polynomials of order ≤ 6.

The equilibrium shape of the sample is symmetric with respect to the vertical axis [22] and hence, its volume is calculated using the following integral:

$$V_{\mathrm{p}} = \frac{2}{3}\pi \int_0^{\pi} \langle R(\varphi)\rangle^3 \sin(\varphi) d\varphi \tag{8}$$

V_{p} is the volume in pixel units. It is related to the real volume V by $V_{\mathrm{p}} = qV$ where q is a scaling factor determined by a calibration using ball bearings. This procedure allows an absolute measurement of the density. The total error was found to be $\Delta\rho/\rho \approx 1.5\%$ [22,23].

For the surface-tension measurement, a C-MOS video camera (400 fps, 1024×1000 pixels) is directed at the sample from the top. A series of 4196 frames is recorded at each temperature and is analyzed afterwards by an edge detection algorithm. The frequency spectrum of the drop radius exhibits a set of five peaks $\omega_{\mathrm{m}}, m = -2, -1, 0, 1, 2$ from which the surface tension is calculated following the sum rule of Cummings and Blackburn [24]:

$$\gamma = \frac{3M}{160\pi} \sum_{m=-2}^{+2} \omega_m^2 - 1.9\Omega^2 - 0.3\left(\frac{g}{a}\right)^2 \Omega^{-2} \tag{9}$$

where M is the mass of the sample, a is its radius, and g is the acceleration of gravity. Ω is calculated from the three translational frequencies $\omega_{\mathrm{X}}, \omega_{\mathrm{Y}}$, and ω_{Z} of the sample, i.e.,

$$\Omega^2 = \frac{1}{3}\left(\omega_X^2 + \omega_Y^2 + \omega_Z^2\right) \tag{10}$$

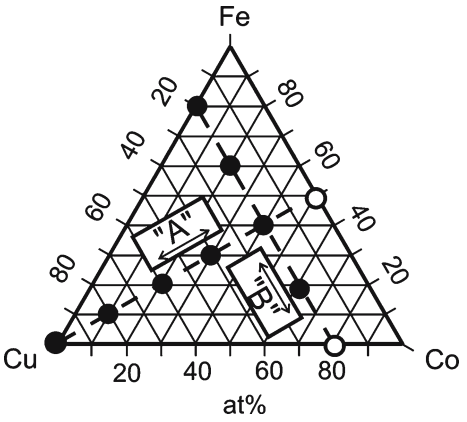

Fig. 1. Concentrations of the investigated samples. Along Section A, the concentration of copper is the main parameter and the ratio c_{Co}: c_{Fe} is 1:1. Along Section B, the concentration of copper is kept constant at 20 at% and the main parameter is the concentration of cobalt which ranges from 0 to 80 at%.

The relative error of the surface tension is approximately $\Delta\gamma/\gamma \approx 5\%$. A more detailed description of the procedure is given, for instance, in Ref. 25.

3. RESULTS AND DISCUSSION

The samples were prepared by melting together the required amounts of the constituent elements in an arc furnace. Figure 1 shows the compositions of the samples that have been investigated marked as dots in the ternary diagram. Two sections through the system, denoted in Fig. 1 as "A" and "B," were investigated. Along Section A, which is summarized by the formula $Cu_xCo_{0.5(1-x)}Fe_{0.5(1-x)}$, the ratio of Co to Fe is 1:1 and the concentration of copper varies from 0 to 100%.

Section B is orthogonal to Section A. It is described by the formula $Cu_{0.2}Co_xFe_{0.8-x}$; the main parameter here is the concentration of Co, which ranges from 0 to 80 at% while the concentration of copper is fixed at 20 at%.

Results for the density $\rho(T)$ and for the surface tension $\gamma(T)$ are shown as an example for Section A in Figs. 2 and 3, respectively. The densities and surface tensions can both be described as linear functions of

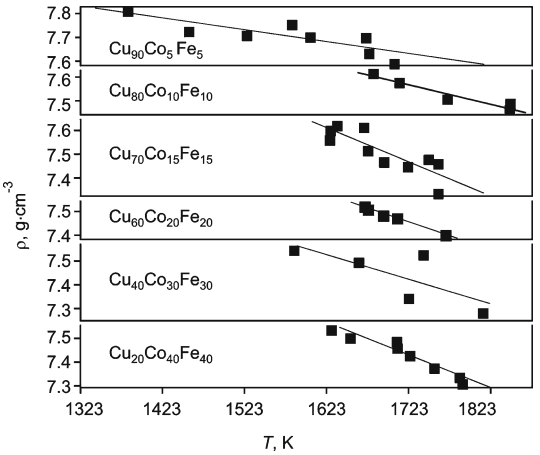

Fig. 2. Density of liquid Cu–Co–Fe samples versus temperature (Section A).

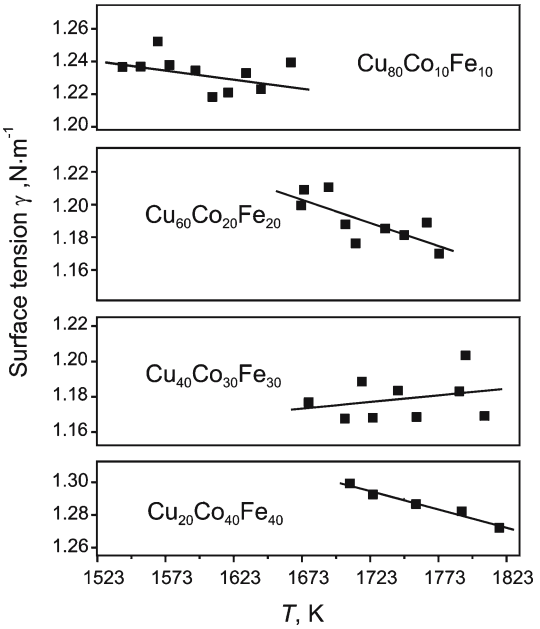

Fig. 3. Surface tension of liquid Cu–Co–Fe samples versus temperature (Section A).

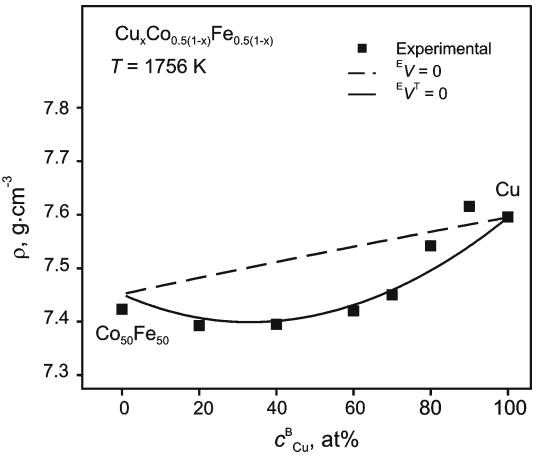

Fig. 4. Density of liquid $Cu_xCo_{0.5(1-x)}Fe_{0.5(1-x)}$ samples (Section A) at 1756 K versus copper concentration. Experimental data are shown together with calculations for $^{E}V = 0$ (dashed line) and $^{E}V_{i,j}$ from Ref. 16 and $^{E}V^{T} = 0$ (solid line).

temperature and hence the following linear relations can be fitted:

$$\rho(T) = \rho_L + \rho_T(T - T_L) \tag{11}$$

$$\gamma(T) = \gamma_L + \gamma_T(T - T_L) \tag{12}$$

In Eq. (11), ρ_L is the density at the liquidus temperature T_L, and ρ_T is the temperature gradient. Similarly in Eq. (12), γ_L is the surface tension at T_L, and γ_T is the temperature gradient of the surface tension. As shown in Fig. 3, γ_T can be either positive or negative.

The fit parameters are listed for Sections A and B in Table I for the density and in Table II for the surface tension.

From the parameters ρ_L and ρ_T in Table I, the density is calculated at $T = 1756$ K so that the concentration dependence can be studied. The result is shown in Fig. 4 for samples along Section A. The densities are all in a range between 7.4 and 7.6 g·cm^{-3} and a clear tendency toward larger values, with an increase of the copper concentration, is observed.

In Fig. 4 the data are plotted together with a calculation for $^{E}V = 0$. They are significantly lower and the excess volume is therefore positive. The experimental data agree well with a calculation for Eq. (2) with $^{E}V^{T} = 0$ and parameters $^{E}V_{i,j}$ from Ref. 16.

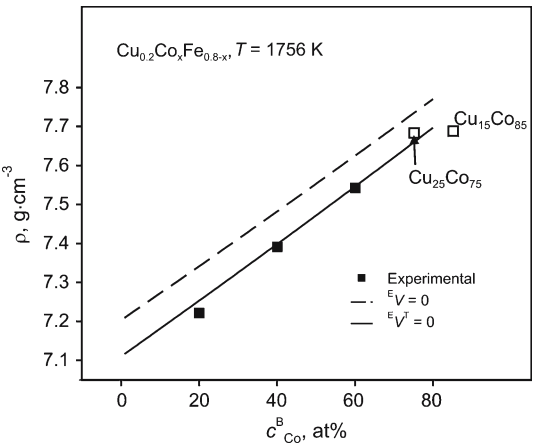

Fig. 5. Density of liquid Cu–Co–Fe samples along Section B at 1756 K versus cobalt concentration. Experimental data are shown together with calculations for ${}^{\mathrm{E}}V = 0$ (dashed line) and ${}^{\mathrm{E}}V_{i,j}$ from Ref. 16 and ${}^{\mathrm{E}}V^{\mathrm{T}} = 0$ (solid line).

Table I. Parameters $T_{\mathrm{L}}, \rho_{\mathrm{L}}, \rho_{\mathrm{T}}$, and $\rho(1756\,\mathrm{K})$ for Ternary Cu–Co–Fe Alloys for Samples along Sections A and B

System	T_{L} (K)	ρ_{L} ($\mathrm{g \cdot cm^{-3}}$)	ρ_{T} ($10^{-4}\,\mathrm{g \cdot cm^{-3} \cdot K^{-1}}$)	$\rho(T = 1756\,\mathrm{K})$ ($\mathrm{g \cdot cm^{-3}}$)
$Co_{50}Fe_{50}$	1752	7.43	−7.48	7.42
$Cu_{20}Co_{40}Fe_{40}$	1696	7.47	−13.7	7.39
$Cu_{40}Co_{30}Fe_{30}$	1675	7.48	−10.3	7.39
$Cu_{60}Co_{20}Fe_{20}$	1662	7.53	−11.7	7.42
$Cu_{70}Co_{15}Fe_{15}$	1656	7.57	−11.5	7.45
$Cu_{80}Co_{10}Fe_{10}$	1639	7.63	−7.79	7.54
$Co_{90}Co_5Fe_5$	1558	7.71	−4.99	7.62
Cu	1358	7.90	−7.65	7.60
$Cu_{20}Co_{20}Fe_{60}$	1711	7.26	−8.39	7.22
$Cu_{20}Co_{40}Fe_{40}$	1696	7.47	−13.7	7.39
$Cu_{20}Co_{60}Fe_{20}$	1693	7.61	−10.5	7.54

The same analysis was performed for Section B in Fig. 5. Here, the data lie on a straight line parallel to the calculation for ${}^{\mathrm{E}}V = 0$. For Section B, the data can also be predicted from Eq. (2), without taking a ternary interaction parameter into account.

The surface tension γ is calculated at $T = 1673\,\mathrm{K}$ from the parameters in Table II and the result of this extrapolation is shown in Fig. 6 for

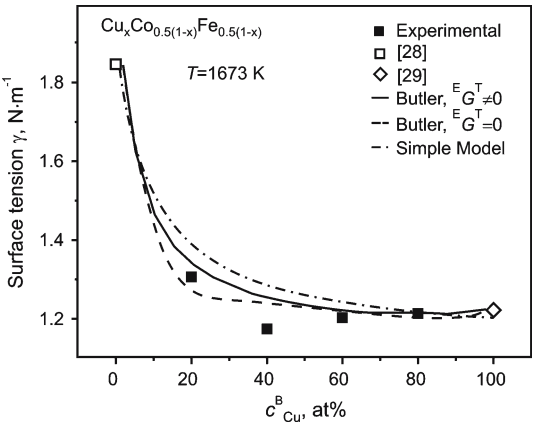

Fig. 6. Surface tension of Cu–Co–Fe samples from Section A at $T = 1673\,\mathrm{K}$ versus copper concentration. Experimental data are shown in comparison with calculations for (a) Butler equation, Eq. (6), with $^{E}G^{T} \neq 0$ (solid line), (b) Butler equation, Eq. (6), with $^{E}G^{T} = 0$ (dashed line), and (c) simple model, Eq. (13), (dashed-dotted line).

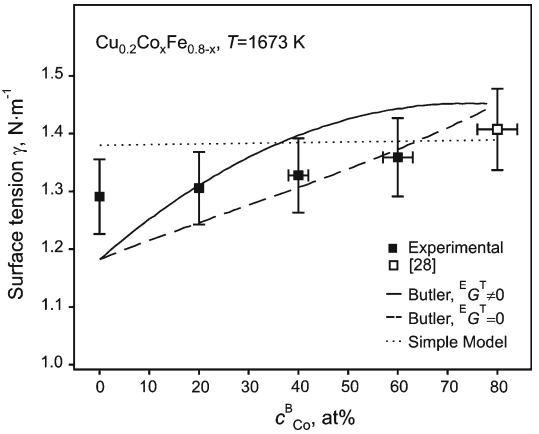

Fig. 7. Surface tension of Cu–Co–Fe samples from Section B at $T = 1673\,\mathrm{K}$ versus cobalt concentration. Experimental data are shown in comparison with calculations for (a) Butler equation, Eq. (6), with $^{E}G^{T} \neq 0$ (solid line), (b) Butler equation, Eq. (6), with $^{E}G^{T} = 0$ (dashed line), and (c) simple model, Eq. (13), (dotted line).

Section A and in Fig. 7 for Section B. Starting in Fig. 6 with $Co_{50}Fe_{50}$ on the left-hand side, the surface tension sharply decreases within the first 20 at% of copper from the initial value of $1.85\,N{\cdot}m^{-1}$ down to approx. $1.3\,N{\cdot}m^{-1}$. It then decreases only slowly until a minimum of $1.2\,N{\cdot}m^{-1}$ is reached at $c^{B}_{Cu} = 40$ at%. On further increase of c^{B}_{Cu}, γ increases again up to $1.25\,N{\cdot}m^{-1}$ where it remains constant until a concentration of 100 at% copper is reached.

For samples along Section B, the surface tensions are shown at 1673 K in Fig. 7. With increasing c^{B}_{Co}, γ appears to be constant at approximately $1.3\,N{\cdot}m^{-1}$.

The data in Figs. 6 and 7 are plotted together with corresponding solutions of the Butler equation, using ${}^{E}G$ (Eq. (5)) once with and once without the ternary interaction term G^{T}. As visible from these figures, both cases agree with our experimental data. With respect to the experimental error, both cases ($G^{T} \neq 0$ and $G^{T} = 0$) describe the surface tension of Cu–Co–Fe equally well.

This shows that the surface tension of Cu–Co–Fe can be predicted from the binary phases without including possible ternary interactions. This result is not unexpected as the actual contribution of the ternary parameter G^{T} is small and the same result is also found for the similar Ni–Cu–Fe system [8,9].

On the other hand, the surface tension, γ, remains constant upon exchange of the two transition metals, Co and Fe, along Section B. Therefore, with respect to the surface tension, the Cu–Co–Fe system can be seen as a binary alloy, where one component is copper and the other component is represented by the two transition metals, Co and Fe.

For the Ni–Cu–Fe system these considerations led to the development of a simple model [8], which can also be applied to Cu–Co–Fe.

In this model, the surface tension is calculated from the ideal solution model:

$$\gamma_{CuCoFe} = c^{S}_{Cu}\gamma_{Cu} + \left(1 - c^{S}_{Cu}\right)\gamma_{CoFe} \tag{13}$$

where γ_{CoFe} is the surface tension of the binary Co_yFe_{1-y} alloy which is given by a linear combination of the surface tensions of Co and Fe. For an ideal solution, the surface concentration c^{S}_{Cu} is related to the bulk concentration c^{B}_{Cu} via the following expression:

$$c^{S}_{Cu} = \frac{c^{B}_{Cu}}{c^{B}_{Cu} + \left(1 - c^{B}_{Cu}\right)\exp\left(A\frac{\gamma_{Cu} - \gamma_{CoFe}}{T}\right)} \tag{14}$$

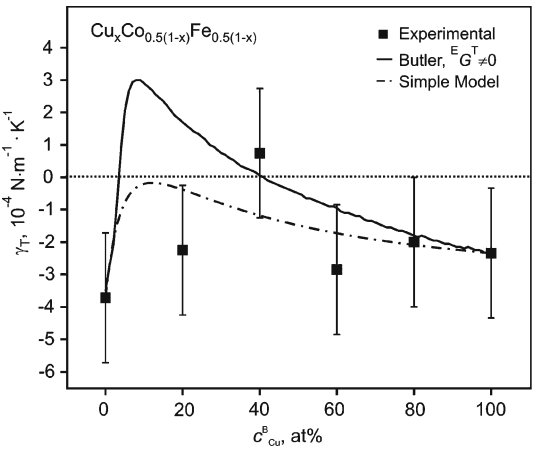

Fig. 8. Temperature coefficient γ_T from Section A versus copper concentration. Experimental data are shown in comparison with calculations for (a) Butler equation, Eq. (6) with ${}^{E}G^{T} \neq 0$ (solid line) and (b) simple model, Eq. (13), (dashed-dotted line).

Table II. Parameters T_L, γ_L, γ_T, and $\gamma(1673\,K)$ for Cu–Co–Fe Alloys of Sections A and B

System	T_L (K)	γ_L ($N \cdot m^{-1}$)	γ_T ($10^{-4}\,N \cdot m^{-1} \cdot K^{-1}$)	$\gamma(T = 1673\,K)$ ($N \cdot m^{-1}$)
$Co_{50}Fe_{50}$	1752	1.82	−3.72	1.85
$Cu_{20}Co_{40}Fe_{40}$	1696	1.30	−2.25	1.31
$Cu_{40}Co_{30}Fe_{30}$	1675	1.17	+0.75	1.17
$Cu_{60}Co_{20}Fe_{20}$	1662	1.21	−2.85	1.20
$Cu_{80}Co_{10}Fe_{10}$	1639	1.22	−2.0	1.21
Cu	1358	1.30	−2.34	1.22
$Cu_{20}Fe_{80}$	1736	1.30	+1.37	1.29
$Cu_{20}Co_{20}Fe_{60}$	1711	1.30	−2.25	1.31
$Cu_{20}Co_{60}Fe_{20}$	1693	1.35	−4.8	1.36
$Cu_{20}Co_{80}$	1698	1.40	−2.0	1.41

In Ref. 8, the factor A in the exponent was set to $6000\,K \cdot mN^{-1}$ and the surface tension of Ni–Cu–Fe was described correctly.

Using the same value, the surface tensions of the Cu–Co–Fe system along Sections A and B are calculated and the results are shown in Figs. 6 and 7. As is obvious, good agreement is obtained in Fig. 6 for Section A. Along Section B, as shown in Fig. 7, the surface tensions predicted by the model are slightly too large.

As seen in Table II, the experimentally obtained temperature coefficient γ_T is positive for $Cu_{20}Fe_{80}$ and $Cu_{40}Co_{30}Fe_{30}$. A positive temperature coefficient was also found experimentally [26] (for $Cu_{18}Fe_{82}$) and theoretically [27] for $Cu_{20}Fe_{80}$. Figure 8 shows a plot of the experimentally obtained temperature coefficient γ_T for ternary alloys of Section A. The experimental values are generally negative except for $Cu_{40}Co_{30}Fe_{30}$. Calculations from the Butler equation, Eq. (6), with ${}^{E}G^{T} \neq 0$ and the simple model, Eq. (13), predict a maximum of γ_T at $c^{B}_{Cu} \approx 20$ at% and the Butler equation even predicts $\gamma_T > 0$ for $10\,\text{at\%} < c^{B}_{Cu} < 40$ at%. The experimental error of $\Delta\gamma_T/\gamma_T$ that is obtained from the fit is approximately 100%. Hence, it is likely that γ_T is positive for $Cu_{40}Co_{30}Fe_{30}$ and $Cu_{10}Co_{15}Fe_{15}$, but it cannot be clearly judged on the basis of the present data.

4. CONCLUSIONS

Density and surface tension data have been measured systematically for the Cu–Co–Fe ternary system. It was shown for the ternary alloys that the density could be derived from the excess volumes of the binary phases without including possible ternary interactions.

The surface tension data are in agreement with solutions of the Butler equation. Similarly to the case for the density, it was found that the surface tension of Cu–Co–Fe could be predicted from the binary phases alone. Moreover, the surface tension was found to be insensitive to the mutual exchange of the two transition metals, Co and Fe. The system could therefore be described as a pseudo-binary alloy of the form Cu–Me, with Me being an arbitrary binary alloy of the transition metals Co and Fe. Comparison with a corresponding model showed good agreement.

ACKNOWLEDGMENT

Financial support by the "Deutsche Forschungsgemeinschaft" under grant number EG 93/4-2 is gratefully acknowledged.

REFERENCES

1. G. Binnach, G. Grünberg, F. Saurenbach, and W. Zinn, *Phys. Rev. B* **39**:4828 (1989).
2. G. Volkova, T. Krieger, L. Plyasova, V. Zaikowskii, and T. Yurieva, *Stud. Surf. Sci. Catal.* **107**:67 (1997).
3. E. Yu Tsymbal and D. G. Pettifor, *J. Magn. Magn. Mater*. **202**:163 (1999).
4. O. Crisan, J. M. Le Breton, A. Jianu, A. Maignan, M. Nogues, J. Teillet, and G. Filoti, *J. Magn. Magn. Mater*. **165**:108 (1997).

5. I. Egry and J. Brillo, *Modelling of Casting, Welding and Advanced Solidification Processes (MCWASP) XI, Proc. TMS* 2006 (2006), pp. 1181–1188.
6. S. Watanabe and T. Saito, *Trans. JIM* **13**:187 (1973).
7. J. Brillo and I. Egry. *J. Mater. Sci*. **40**:2213 (2005).
8. I. Egry, J. Brillo, and T. Matsushita, *Mater. Sci. Eng. A* **413–414**:460 (2005).
9. J. Brillo, I. Egry, and T. Matsushita, *Z. Metallkd*. **97**:28 (2006).
10. S. Bein, C. Colinet, and M. Durand-Charre, *J. Alloy Compd*. **313**:133 (2000).
11. D. I. Kim and R. Abbaschian, *J. Phase Equilib*. **21**:133 (2000).
12. M. Bamberger, A. Munitz, L. Kaufman, and R. Abbaschian, *Calphad* **26**:375 (2002).
13. C. Chong-De and G. P. Görler, *Chin. Phys. Lett*. **22**:482 (2005).
14. C. Lüdecke and D. Lüdecke, *Thermodynamik* (Springer, Heidelberg, 2000).
15. H. D. Baehr, *Thermodynamik* (Springer, Heidelberg, 2002).
16. J. Brillo, I. Egry, and T. Matsushita, *Int. J. Mater. Res*. **97**:11 (2006).
17. J. A. V. Butler, *Proc. Roy. Soc*. **135 A**:348 (1932).
18. T. Tanaka and T. Iida, *Steel Res*. **65**:211 (1994).
19. R. S. Schmid-Fetzer and J. Gröbner, *Adv. Eng. Mater*. **3**:947 (2001).
20. M. Hillert, *Calphad* **4**:1 (1980).
21. C. Servant, B. Sundman, and O. Lyon, *Calphad* **25**:79 (2001).
22. J. Brillo and I. Egry, *Int. J. Thermophys*. **24**:1155 (2003).
23. J. Brillo, I. Egry, and I. Ho, *Int. J. Thermophys*. **27**:494 (2006).
24. D. L. Cummings and D. A. Blackburn, *J. Fluid Mech*. **224**:395 (1991).
25. S. Schneider, I. Egry, and I. Seyhan, *Int. J. Thermophys*. **23**:1241 (2002).
26. J. Xu, Z. Qiao, X. Han, B. Wei, J. Lee, and T. Tanaka, *Z. Metallkd*. **95**:1001 (2004).
27. D. Chatain, *private communication*.
28. R. Eichel and I. Egry, *Z. Metallkd*. **90**:5 (1999).
29. S. Sauerland, K. Eckler, and I. Egry, *Mater. Sci. Lett*. **11**:330 (1992).